Chinese Physics B

PAPER

Microwave field sensor based on cold cesium Rydberg three-photon electromagnetically induced spectroscopy

To cite this article: Yuan-Yuan Wu *et al* 2024 *Chinese Phys. B* **33** 113201

Microwave field sensor based on cold cesium Rydberg three-photon electromagnetically induced spectroscopy

Yuan-Yuan Wu(吴圆圆)[1], Yun-Hui He(何云辉)[1], Yue-Chun Jiao(焦月春)[1,2,†], and Jian-Ming Zhao(赵建明)[1,2,‡]

[1] *State Key Laboratory of Quantum Optics and Quantum Optics Devices, Institute of Laser Spectroscopy, Shanxi University, Taiyuan* 030006, *China*
[2] *Collaborative Innovation Center of Extreme Optics, Shanxi University, Taiyuan* 030006, *China*

(Received 2 July 2024; revised manuscript received 28 August 2024; accepted manuscript online 30 August 2024)

We present the electromagnetically induced transparency (EIT) spectra of cold Rydberg four-level cascade atoms consisting of the $6S_{1/2} \rightarrow 6P_{3/2} \rightarrow 7S_{1/2} \rightarrow 60P_{3/2}$ scheme. A coupling laser drives the Rydberg transition, a dressing laser couples two intermediate levels and a weak probe laser probes the EIT signal. We numerically solve the Bloch equations and investigate the dependence of the probe transmission rate signal on the coupling and dressing lasers. We find that the probe transmission rate can display an EIT or electromagnetically induced absorption (EIA) profile, depending on the Rabi frequencies of the coupling and dressing lasers. When we increase the Rabi frequency of the coupling laser and keep the Rabi frequency of the probe and dressing laser fixed, flipping of the EIA to EIT spectrum occurs at the critical coupling Rabi frequency. When we apply a microwave field coupling the transition $60P_{3/2} \rightarrow 61S_{1/2}$, the EIT spectrum shows Autler–Townes splitting, which is employed to measure the microwave field. The theoretical measurement sensitivity can be 1.52×10^{-2} nV·cm^{-1}·Hz$^{-1/2}$ at the EIA–EIT flipping point.

Keywords: Rydberg atoms, atomic microwave sensor, electromagnetically induced transparency and absorption

PACS: 32.80.Ee, 32.30.Bv, 42.50.Gy **DOI:** 10.1088/1674-1056/ad7579

1. Introduction

The electromagnetically induced transparency (EIT) of Rydberg three-level atoms has been widely investigated due to its non-destructive detection of Rydberg levels and potential application in microwave measurement. Rydberg atoms, with principal quantum number larger than 10, exhibit unique properties,[1,2] such as high polarizability ($\sim n^{*7}$, with n^* the effective quantum number) and a large microwave transition dipole moment ($\sim n^{*2}$), making them extremely sensitive to the external electric field.[3] Rydberg EIT exhibits Autler–Townes (AT) splitting[4,5] or Stark shifts[6–8] when an external field is applied that interacts with the Rydberg atom; this has been employed to realize calibration-free microwave field measurements covering a wide frequency range from about 1 GHz to 1 THz,[9–12] including measurement of the radio-frequency field strength,[13–15] polarization[16,17] and phase,[18–20] as well near-field terahertz imaging[12] and subwavelength microwave imaging.[21,22] When using the Rydberg EIT–AT splitting method as a field sensor, the sensitivity of a Rydberg atom can be 30 μV·cm^{-1}·Hz$^{-1/2}$.[9] With implementation of the Rydberg atomic heterodyne technique,[17,23,24] the sensitivity of Rydberg atom receivers has been significantly enhanced to 55 nV·cm^{-1}·Hz$^{-1/2}$[18] and later to 30 nV·cm^{-1}·Hz$^{-1/2}$.[25]

All the above applications are based on the Rydberg three-level two-photon EIT scheme, and the related EIT resonance linewidth is limited by the Doppler mismatch between the probe and coupling lasers. The four-level three-photon scheme can effectively cancel the Doppler mismatch and decrease the EIT linewidth. Furthermore, this scheme requires three semiconductor lasers, which are cheap and simple structures with high stability. Four-level spectroscopy demonstrates the feature of flipping of electromagnetically induced absorption (EIA) to EIT, which can be employed to detect the microwave field. Four-level EIT has already been investigated.[26–29] Thaicharoen *et al.*[28] theoretically investigated EIT and EIA spectroscopy and microwave-field sensing with a Rb vapor cell. Nikunjkumar *et al.*[29] used a cesium four-level atom with the 9S intermediate state to obtain an EIT linewidth of 39 kHz. Their results showed that for a probe Rabi frequency larger than three-fifths of the coupling Rabi frequency the EIA flips to EIT. The three-photon system can lead to narrower resonances; however, this does not necessarily translate directly to optimal conditions for field sensitivity.

In this work, we focus on the four-level cold cesium atomic system formed with the $6S_{1/2} \rightarrow 6P_{3/2} \rightarrow 7S_{1/2} \rightarrow 60P_{3/2}$ scheme. We numerically solve the Bloch equation and investigate the EIT and EIA effects of four-level atoms. Cold atoms with a temperature of ~ 100 μK have a long coherence time, yielding narrow-linewidth EIT. The dependence of EIT transmission on the Rabi frequency of the dressing and coupling lasers is investigated. The EIT transmission signal decreases with coupling Rabi frequency and converts to an EIA signal at critical coupling Rabi frequency, at which point the

†Corresponding author. E-mail: ycjiao@sxu.edu.cn
‡Corresponding author. E-mail: zhaojm@sxu.edu.cn

probe transition is sensitive to the microwave field; this can be used to measure the microwave field with improved sensitivity.

2. Theoretical model

We consider a four-level ladder cesium atom with a ground state $|6S_{1/2}\rangle$, two intermediate states $|6P_{3/2}\rangle$ and $|7S_{1/2}\rangle$ and Rydberg state $|60P_{3/2}\rangle$ (see Fig. 1). The first photon of an 852 nm laser, a weak probe laser, drives the lower transition $|6S_{1/2}\rangle \to |6P_{3/2}\rangle$ with a detuning Δ_p and a Rabi frequency $\Omega_p/2\pi = 3$ MHz. The second photon of a 1470 nm laser, a dressing laser, couples the middle transition

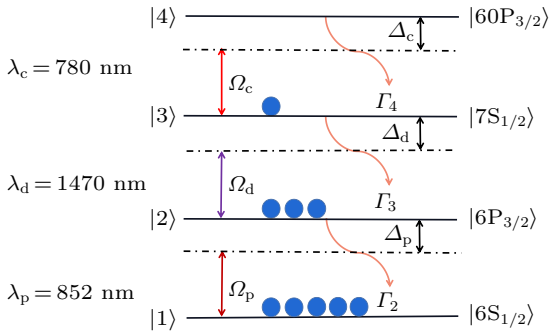

Fig. 1. Energy level diagram of the cesium cascade four-level system. A weak probe laser ($\lambda_p = 852$ nm, Rabi frequency Ω_p) couples the transition $|6S_{1/2}\rangle(|1\rangle) \to |6P_{3/2}\rangle(|2\rangle)$. The dressing laser ($\lambda_d = 1470$ nm, Ω_d) drives the transition of two intermediate states, $|6P_{3/2}\rangle(|2\rangle) \to |7S_{1/2}\rangle(|3\rangle)$. The coupling laser ($\lambda_c = 780$ nm, Ω_c) is scanned over the Rydberg transition, $|7S_{1/2}\rangle(|3\rangle) \to 60P_{3/2}\rangle(|4\rangle)$. Γ_i $(i = 2,3,4)$ denotes the decay of excited states $|i\rangle$. Δ_p, Δ_d and Δ_c display the detuning of the probe, dressing and coupling lasers, respectively.

$|6P_{3/2}\rangle \to |7S_{1/2}\rangle$ with a Rabi frequency Ω_d and fixed detuning $\Delta_d = 0$ MHz. The third photon of a 780 nm laser, a coupling laser, achieves Rydberg excitation of the up transition $|7S_{1/2}\rangle \to |60P_{3/2}\rangle$ with detuning Δ_c and a Rabi frequency of Ω_c.

The Hamiltonian of a four-level system can be expressed as

$$H = \frac{\hbar}{2}\begin{pmatrix} 0 & \Omega_p & 0 & 0 \\ \Omega_p & -2\Delta_1 & \Omega_d & 0 \\ 0 & \Omega_d & -2\Delta_2 & \Omega_c \\ 0 & 0 & \Omega_c & -2\Delta_3 \end{pmatrix}, \tag{1}$$

where Δ_1, Δ_2 and Δ_3 can be written as

$$\begin{aligned} \Delta_1 &= \Delta_p, \\ \Delta_2 &= \Delta_p + \Delta_d, \\ \Delta_3 &= \Delta_p + \Delta_d + \Delta_c. \end{aligned} \tag{2}$$

Considering the decay of the system, the Lindblad equation is used to describe the evolution of the density matrix ρ as follows:

$$\dot{\rho} = -\frac{\mathrm{i}}{\hbar}[H,\rho] + \mathcal{L}, \tag{3}$$

where $\mathcal{L}$ is the Lindblad operator that indicates the decay processes of atoms

$$\mathcal{L} = \begin{pmatrix} \Gamma_2\rho_{22} & -\frac{1}{2}\Gamma_2\rho_{12} & -\frac{1}{2}\Gamma_3\rho_{13} & -\frac{1}{2}\Gamma_4\rho_{14} \\ -\frac{1}{2}\Gamma_2\rho_{21} & -\Gamma_2\rho_{22} + \Gamma_3\rho_{33} & -\frac{1}{2}(\Gamma_2+\Gamma_3)\rho_{23} & -\frac{1}{2}(\Gamma_2+\Gamma_4)\rho_{24} \\ -\frac{1}{2}\Gamma_3\rho_{31} & -\frac{1}{2}(\Gamma_2+\Gamma_3)\rho_{32} & -\Gamma_3\rho_{33} + \Gamma_4\rho_{44} & -\frac{1}{2}(\Gamma_3+\Gamma_4)\rho_{34} \\ -\frac{1}{2}\Gamma_4\rho_{41} & -\frac{1}{2}(\Gamma_2+\Gamma_4)\rho_{42} & -\frac{1}{2}(\Gamma_3+\Gamma_4)\rho_{43} & -\Gamma_4\rho_{44} \end{pmatrix}. \tag{4}$$

For convenience, $\{|1\rangle, |2\rangle, |3\rangle, |4\rangle\}$ is used as the state basis to represent $\{|6S_{1/2}\rangle, |6P_{3/2}\rangle, |7S_{1/2}\rangle, |60P_{3/2}\rangle\}$. ρ_{kj} is the density matrix element with $k, j \in \{1,2,3,4\}$. Γ_i $(i = 2,3,4)$ denotes the spontaneous decay rate of the $|i\rangle$ state. Here the dephasing effects due to the laser linewidth, transition broadening and collisions between atoms are not considered. For cesium atoms, we take the decay rates $\Gamma_2 = 2\pi \times 5.22$ MHz, $\Gamma_3 = 2\pi \times 3.29$ MHz and $\Gamma_4 = 2\pi \times 0.76$ kHz, respectively. The weak probe laser is locked to the transition $|1\rangle \to |2\rangle$, the dressing laser is locked to the resonant transition $|2\rangle \to |3\rangle$ and the strong coupling laser scans over the Rydberg transition $|3\rangle \to |4\rangle$, then we set $\Delta_d = 0$ MHz in calculations.

For the atomic system, the probe transmission rate is defined as $\mathcal{R} = P/P_{in} = \exp(-\alpha L)$, where P_{in} is the probe power before the cell and L is the length of our atomic cloud. The parameter $\alpha = 2\pi\,\mathrm{Im}(\chi)/\lambda_p$ is the absorption coefficient of the probe laser based on Beer's law, with χ the susceptibility of the medium. The susceptibility χ is written as[30]

$$\chi = \frac{2N\mu_{12}}{E_p\varepsilon_0}\rho_{12}, \tag{5}$$

where μ_{12} is the dipole moment of the transition $|1\rangle \to |2\rangle$, E_p is the amplitude of the probe laser field, ε_0 is the vacuum permittivity, N is an atomic density and ρ_{12} is the density matrix element in Eq. (3). The average atomic density is $N = 10^{10}$ cm^{-3} at temperature $T \simeq 100$ μK for a typical cold cloud of $L = 2.5$ mm, the corresponding velocity of the atoms is a few cm·s^{-1} leading to negligible Doppler broadening. Note that when the system is at room temperature ($T = 300$ K), the Doppler broadening and shift can no longer

be neglected. The laser direction and Doppler shifts for probe and coupling and dressing lasers should be included.

3. Results and discussion

We numerically solve Eq. (3) and obtain ρ_{12} and the probe transmission rate $\mathcal{R}$. Here we keep $\Delta_p = 0$ MHz and $\Delta_d = 0$ MHz and scan the coupling laser frequency over the Rydberg transition to investigate the probe transmission rate as a function of the dressing and coupling Rabi frequencies. If the probe transmission rate is positive, the atomic system is in the EIT regime, whereas if the probe transmission rate is negative the atomic system is in the EIA regime.

3.1. The Ω_d dependence

In this section, we investigate the dependence of the probe transmission rate on the Rabi frequency of the dressing laser Ω_d and keep the $\Omega_p/2\pi = 3$ MHz and $\Omega_c/2\pi = 1$ MHz. Figure 2 presents the calculation of the probe transmission rate for $\Omega_d/2\pi = 10$ MHz (Fig. 2(a)) and $\Omega_d/2\pi = 30$ MHz (Fig. 2(b)). It is seen that the probe transmission rate shows that the EIT spectra and EIT signal are about three times larger for $\Omega_d/2\pi = 10$ MHz than for $\Omega_d/2\pi = 30$ MHz. In order to understand the variation of the EIT signal, we perform a series of calculations for the range $\Omega_d/2\pi = 0.5$–50 MHz. Figure 3(a) plots the EIT spectra as a function of the coupling detuning Δ_c and the dressing laser Rabi frequency Ω_d, with $\Omega_p/2\pi = 3$ MHz and $\Omega_c/2\pi = 1$ MHz. Figure 3(b) displays the EIT transmission and linewidth, extracted by Lorentz fitting to the spectra, as a function of Ω_d. It is found that the EIT transmission rate increases with the Rabi frequency of the dressing laser up to a maximum when $\Omega_d/2\pi = 10.52$ MHz. When we further increase Ω_d, the EIT transmission rate begins to decrease. In addition, the EIT linewidth decreases with Ω_d; the linewidth can be 0.25 MHz at $\Omega_d/2\pi = 40$ MHz.

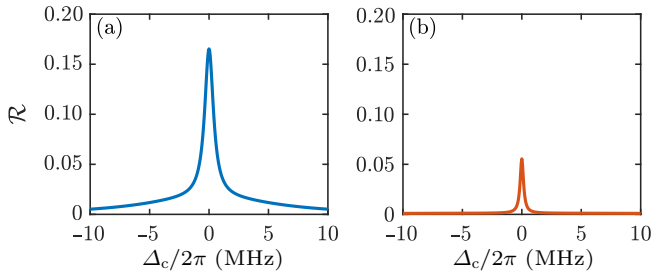

Fig. 2. EIT spectra as a function of the coupling detuning Δ_c, with $\Omega_{p,d,c}/2\pi = 3$ MHz, 10 MHz and 1 MHz in (a) and $\Omega_{p,d,c}/2\pi = 3$ MHz, 30 MHz and 1 MHz in (b).

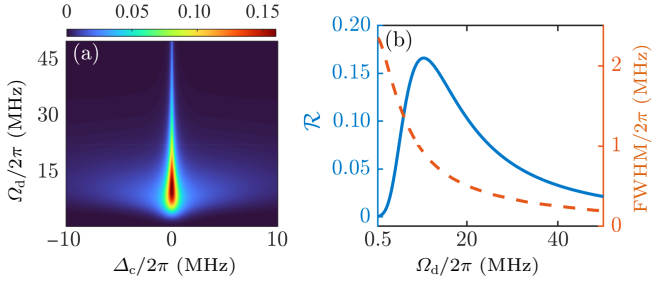

Fig. 3. (a) Calculations of EIT spectra as a function of the coupling detuning Δ_c and the Rabi frequency of the dressing laser Ω_d, with $\Omega_p/2\pi = 3$ MHz and $\Omega_c/2\pi = 1$ MHz. (b) EIT transmission rate (blue solid line) with $\Delta_c = 0$ MHz and full-width at half-maximum (FWHM) (orange dashed line) of the EIT spectra in (a) as a function of Ω_d. The EIT transmission rate shows an increase with Ω_d up to a maximum when $\Omega_d/2\pi = 10.52$ MHz. When Ω_d is further increased the EIT transmission rate decreases with Ω_d. The linewidth shows a decrease with Ω_d.

3.2. The Ω_c dependence

We next investigate the dependence of the probe transmission rate on the Rabi frequency of the coupling laser Ω_c and keep $\Omega_p/2\pi = 3$ MHz and $\Omega_d/2\pi = 10$ MHz. Figures 4(a) and 4(b) present the probe transmission rate spectra as a function of coupling laser detuning for $\Omega_c/2\pi = 1$ MHz and $\Omega_c/2\pi = 7$ MHz, respectively. It is interesting to see that the EIT spectrum for $\Omega_c/2\pi = 1$ MHz of Fig. 4(a) flips to the EIA spectrum for $\Omega_c/2\pi = 7$ MHz of Fig. 4(b). This phenomenon can be explained by the fact that the coherence between the excited state $|3\rangle$ and the Rydberg state $|4\rangle$ is broken due to the strong coupling of the coupled laser, which results in an increase in the absorption encountered by the probe laser as it passes through the medium, forming the EIA spectrum.[27,31]

To explain what happens when the coupling Rabi frequency increases and to explore the flip point, we carried out more calculations of probe transmission rate spectra by varying the Rabi frequency of the coupling laser from $\Omega_c/2\pi = 0.5$ MHz to 15 MHz while keeping $\Omega_p/2\pi = 3$ MHz and $\Omega_d/2\pi = 10$ MHz fixed. From the EIT or EIA spectra, we extracted the peak amplitude and plotted it as a function of the coupling Rabi frequency, as shown by the blue solid line in Fig. 4(c). It is found that the probe transmission displays an EIT spectrum when $\Omega_c/2\pi < 2.61$ MHz but an EIA spectrum when $\Omega_c/2\pi > 2.61$ MHz. The Rabi frequency of the coupling laser $\Omega_c/2\pi = 2.61$ MHz is the critical point at which EIT flips to EIA for cesium four-level atoms. To verify the ubiquity of EIT–EIA flipping, the Rabi frequency of the dressing laser $\Omega_d/2\pi = 30$ MHz was changed and similar calculations to Figs. 4(a) and 4(b) were performed. The probe transmission rate amplitude as a function of Ω_c is plotted by the orange dash-dotted line in Fig. 4(c). Note that (i) the probe transmission rate amplitude is smaller for large Rabi frequencies of the dressing laser ($\Omega_d/2\pi = 30$ MHz) than for small ones ($\Omega_d/2\pi = 10$ MHz). This may be because the larger dressing field leads to decoherence of the four-level atomic system, which agrees with the calculation in Fig. 3(b). (ii) The probe transmission rate spectra display a similar phenomenon of EIT–EIA flipping when the Rabi frequency of the coupling laser Ω_c is increased and the critical flipping point appears at about the same point. The inset to Fig. 4(c) displays a zoomed-in view of the critical point marked with a shaded square, from which we extract the critical point as 2.38 MHz for $\Omega_d/2\pi = 30$ MHz.

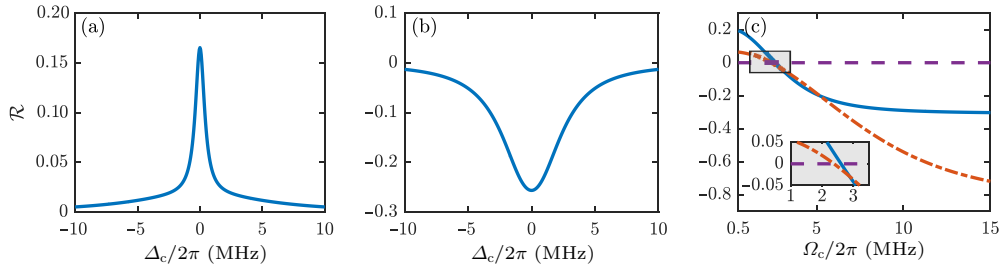

Fig. 4. The probe transmission spectra with fixed $\Omega_p/2\pi = 3$ MHz and $\Omega_d/2\pi = 10$ MHz and for different coupling Rabi frequencies: (a) $\Omega_c/2\pi = 1$ MHz and (b) $\Omega_c/2\pi = 7$ MHz. The probe spectrum displays an EIT profile in (a) and EIA in (b). (c) Peaks of the probe transmission rate as a function of the coupling Ω_c for $\Omega_d/2\pi = 10$ MHz (blue solid line) and 30 MHz (orange dash-dotted line). The inset is a zoomed-in view near the critical point, marked with a shaded square. The critical coupling Rabi frequencies are 2.61 MHz and 2.38 MHz for $\Omega_d/2\pi = 10$ MHz and 30 MHz, respectively. The horizontal dashed line marks $\mathcal{R} = 0$.

Detailed analysis of the theoretical calculations for parameters Ω_p, Ω_d and Ω_c indicates that small changes in Ω_p, large changes in Ω_c or even larger changes in Ω_d can flip the EIA and EIT lines. Next, we consider the flipping of EIA to EIT by changing Ω_c as an example and explore microwave measurements based on four-level atoms.

3.3. Microwave measurements

Rydberg three-level EIT in microwave fields can split and form EIT–AT splitting spectra, which are employed to realize calibration-free microwave measurement.[9] For the four-level EIT in this work, the EIT signal also displays AT splitting when we apply a microwave field coupling the Rydberg transition (see Fig. 5(b)), where the microwave field (Ω_{mw}) couples the Rydberg transition $|60P_{3/2}\rangle \rightarrow |61S_{1/2}\rangle$. We solve the matrix density equation of a five-level atom with $\Gamma_5/2\pi = 0.71$ kHz. Figure 5(c) presents the calculated EIT spectra with and without a microwave field, in which the field-free probe transmission rate spectrum displays the EIT profile for $\Omega_{p,d,c}/2\pi = 3$ MHz, 10 MHz and 1 MHz. The probe transmission rate displays the typical EIT spectrum in the absence of a microwave field and EIT–AT splitting with a microwave field of $\Omega_{mw}/2\pi = 2$ MHz. The measured EIT–AT splitting is proportional to the microwave Rabi frequency Ω_{mw}, which is similar to three-level EIT[9] and can also be used to measure the microwave field.

As mentioned above, there is a critical point for flipping EIA to EIT for the four-level atom (see Fig. 4(c)). The simulation shows that the flipping of EIA to EIT occurs when a weak microwave field is applied near the critical parameter with $\Omega_{p,d,c}/2\pi = 3$ MHz, 10 MHz and 2.65 MHz, as shown in Fig. 6(a). It is seen that the probe transmission rate displays the EIA profile in the absence of a microwave field (blue dashed line in Fig. 6(a)) and the EIT profile when a microwave field is applied (yellow dot-dashed and orange solid lines of Fig. 6(a) for $\Omega_{mw}/2\pi = 0.5$ MHz and 0.05 MHz, respectively). When we further increase Ω_{mw}, the EIT signal shows AT splitting, as shown in Fig. 5(c).

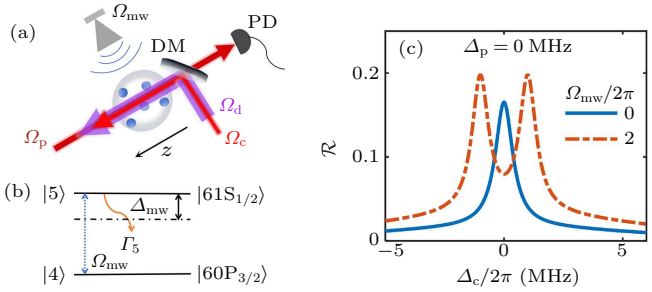

Fig. 5. (a) Sketch of the experimental setup. The coupling and dressing lasers co-propagate along the z-axis, whereas the probe laser is set to counter-propagate relative to the coupling and dressing beams through the center of the cesium cold atoms. The microwave field is emitted by a horn antenna perpendicular to the z-axis. PD, photodiode; DM, dichroic mirror. (b) Schematic diagram of the microwave dressed Rydberg transition $|60P_{3/2}\rangle \rightarrow |61S_{1/2}\rangle$. (c) EIT–AT spectra for $\Omega_{p,d,c}/2\pi = 3$ MHz, 10 MHz and 1 MHz and indicated microwave Rabi frequencies of $\Omega_{mw}/2\pi = 0$ (blue solid line) and 2 MHz (orange dash-dotted line). Similar to three-level EIT, microwave-coupled EIT–AT splitting can be used to measure the microwave field.

To explore the evolution of EIA to EIT near the critical point, a series of calculations were done by changing the microwave field $\Omega_{mw}/2\pi = 0$–10 MHz and extracting the EIT or EIA amplitude. Figure 6(b) displays the peak of the probe transmission rate $\mathcal{R}$ as a function of Ω_{mw}. $\mathcal{R}$ shows EIA in the absence of a microwave field; the EIA signal decreases when a microwave field is applied and disappears when $\Omega_{mw}/2\pi = 0.0049$ MHz, meaning that the EIA spectrum converts to an EIT spectrum. When $\Omega_{mw}/2\pi = 0.18$ MHz, the amplitude of EIT reaches a maximum.

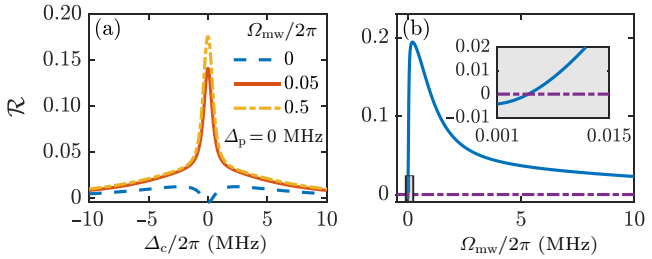

Fig. 6. (a) Probe transmission rate spectra with and without a microwave field near the critical point of flipping from EIA to EIT, with $\Omega_{p,d,c}/2\pi = 3$ MHz, 10 MHz and 2.65 MHz. The transmission rate displays the EIA spectrum (blue dashed line) in the absent of field, but shows the EIT spectrum when a weak microwave field of $\Omega_{mw}/2\pi = 0.05$ MHz (orange solid line) or 0.5 MHz (yellow dot-dashed line) is applied. (b) The peak of EIT or EIA of the probe transition rate at $\Delta_c/2\pi = 0$ MHz as a function of the microwave field Ω_{mw}. The inset displays an enlargement near the flipping point, marked with a shaded square.

It is worth noting that the probe transmission rate includes two regimes, one is the EIA–EIT flipping and EIT increasing regime and the other is the EIT decreasing regime. The latter is also the EIT–AT regime, where the probe spectra show EIT–AT splitting as in Fig. 5(c), similar to the three-level atom, and can be used to measure the microwave field based on EIT–AT splitting.[9] For the first regime, the probe transmission rate displays flipping of EIA to EIT in a very weak microwave field, where variation of the probe transmission rate is very sensitive to the microwave field; this can be employed to precisely measure or sense the microwave field. The inset of Fig. 6(b) shows an enlargement of the flipping point.

Next, we take Fig. 6(b) as an example to illustrate weak microwave measurement based on EIA–EIT flipping. As stated above, near the EIA–EIT flipping point the gradient of the probe transmission rate is huge. The measurement of microwave field transfer to measure the variation of probe transmission rate ($\Delta\mathcal{R}$) when a microwave field is applied, as shown in the inset of Fig. 6(b). The minimum measurable field depends on the minimum change that can be detected in the probe transmission rate ($\Delta\mathcal{R}_{\rm min}$), which is limited by the noise of the system. For an atomic system interacting with the laser beam, the noise limitation is the shot noise of probe beam. The minimum field, $E_{\rm min}$, can be obtained when $\Delta\mathcal{R}_{\rm min}$ becomes indistinguishable from the noise. The shot noise is usually written as $\sigma=\sqrt{n}$ (n is the photon number of probe laser).[32] The noise power for a collection time of 1 s then reads

$$P_{\rm noise}=\sigma h\nu, \tag{6}$$

where h is Planck's constant and ν is probe laser frequency. When the probe transmission change $\Delta P_{\rm out}$ is equal to the noise power $\Delta P_{\rm out}=P_{\rm in}\Delta\mathcal{R}_{\rm min}=P_{\rm noise}$, the corresponding transmission is the minimum resolvable probe transmission rate $\Delta\mathcal{R}_{\rm min}=P_{\rm noise}/P_{\rm in}=\sqrt{h\nu/P_{\rm in}}$. The minimum microwave field that can be detected is written as

$$E_{\rm mw_{min}}=\Omega_{\rm mw_{min}}\hbar/\mu, \tag{7}$$

where $\Omega_{\rm mw_{min}}$ is the minimum microwave Rabi frequency, and can be obtained from $\Delta\mathcal{R}_{\rm min}$ and the maximum slope $(\Delta\mathcal{R}/\Delta\Omega_{\rm mw})_{\rm max}$. For the probe laser Rabi frequency we used, $\Delta\mathcal{R}_{\rm min}=1.008\times10^{-6}$, the minimum measurable microwave Rabi frequency was $\Omega_{\rm mw_{min}}/2\pi=0.245$ Hz, corresponding to a theoretical sensing sensitivity of $S=1.52\times10^{-2}$ nV·cm^{-1}·Hz$^{-1/2}$ for a measurement time of 1 s, which is two orders of magnitude better than the measurement value of 5.1 nV·cm^{-1}·Hz$^{-1/2}$.[33] However, it should be noted that the minimum detected microwave field is limited by the shot noise of the probe laser, which can be decreased by decreasing the power of the probe laser. Weak laser power may lead to a low signal-to-noise ratio of the EIT signal. In the experiments there must be a balance between the probe laser shot noise and the signal-to-noise ratio of the probe transmission rate spectrum. In addition to the shot noise of probe laser, the noise of the coupling laser and frequency fluctuations, etc., also increase the noise limit $P_{\rm noise}$, making sensitivity of the actual measurement lower than suggested by calculations.

The cold atomic system studied in this work has a long coherence time, resulting in narrow linewidth EIT spectroscopy, and the minimum measurable field and sensitivity are two orders of magnitude better than in a vapor cell with the same level scheme. Figure 5(a) presents an experimental protocol for measuring the microwave field, where the cesium atoms are laser-cooled and trapped in a standard magneto-optical trap and the photodiode detector measures the three-photon EIT and EIA spectra and also senses the microwave field.

4. Conclusion

In this work, we investigated the quantum effect of a laser interacting with a cesium four-level cascade atom in theory. By numerically resolving the Hamiltonian equation, we obtained the probe transmission rate as a function of the coupling laser detuning for different Rabi frequencies of $\Omega_{\rm p,d,c}$ and found that probe transmission rate spectra can be converted from EIA to EIT at critical parameters of laser Rabi frequency. By analyzing the probe transmission rate, we extract the critical point. In both the EIT and EIA regimes, the probe transmission rate can lead to AT splitting when we apply a microwave field coupling the Rydberg transition, for example the $|60{\rm P}_{3/2}\rangle\rightarrow|61{\rm S}_{1/2}\rangle$ transition in this work, and the corresponding AT splitting is proportional to the microwave Rabi frequency (see Fig. 5(c)), which is used to measure the microwave field. Importantly, in the regime of EIA–EIT flipping, the EIA signal is converted to an EIT signal with a huge slope when a weak microwave field is applied (see Fig. 6(b)). The EIA–EIT flipping and the huge slope are very sensitive to the microwave field, therefore providing a method to detect the microwave field with high sensitivity. The minimum microwave field obtained depends on the minimum change in the probe transmission rate, and is limited by the shot noise. This work was done within cesium atoms with a temperature of 100 μK, and could easily be extended to the room-temperature case with the Doppler shift included. The investigations in this work are significant for Rydberg atom-based microwave measurement and field sensors.

Acknowledgements

Project supported by the National Natural Science Foundation of China (Grant Nos. U2341211, 62175136, 12241408, and 12120101004), the Innovation Program for Quantum

Science and Technology (Grant No. 2023ZD0300902), the Fundamental Research Program of Shanxi Province (Grant No. 202303021224007), and the 1331 Project of Shanxi Province.

References

[1] Gallagher T F 1994 *Rydberg Atoms* (Cambridge: Cambridge University Press)
[2] Scully M O and Zubairy M S 1997 *Quantum Optics* (Cambridge: Cambridge University Press)
[3] Comparat D and Pillet P 2010 *J. Opt. Soc. Am. B* **27** A208
[4] Autler S H and Townes C H 1955 *Phys. Rev.* **100** 703
[5] Tanasittikosol M, Pritchard J D, Maxwell D, Gauguet A, Weatherill K J, Potvliege R M and Adams C S 2011 *J. Phys. B: At. Mol. Opt. Phys.* **44** 184020
[6] Delone N B and Krainov V P 1999 *Phys. Usp.* **42** 669
[7] Ma L, Viray M A, Anderson D A and Raithel G 2022 *Phys. Rev. Appl.* **18** 024001
[8] Anderson D A, Miller S A, Raithel G, Gordon J A, Butler M L and Holloway C L 2016 *Phys. Rev. Appl.* **5** 034003
[9] Sedlacek J A, Schwettmann A, Kübler H, Löw R, Pfau T and Shaffer J P 2012 *Nat. Phys.* **8** 819
[10] Pritchard J D, Maxwell D, Gauguet A, Weatherill K J, Jones M P A and Adams C S 2010 *Phys. Rev. Lett.* **105** 193603
[11] Chen S Y, Reed D J, MacKellar A R, Downes L A, Almuhawish N F A, Jamieson M J, Adams C S and Weatherill K J 2022 *Optica* **9** 485
[12] Wade C G, Šibalić N, De Melo N R, Kondo J M, Adams C S and Weatherill K J 2017 *Nat. Photon.* **11** 40
[13] Fan H Q, Kumar S, Sedlacek J, Kübler H, Karimkashi S and Shaffer J P 2015 *J. Phys. B: At. Mol. Opt. Phys.* **48** 202001
[14] Jiao Y C, Han X X, Yang Z W, Li J K, Raithel G, Zhao J M and Jia S T 2016 *Phys. Rev. A* **94** 023832
[15] Liu B, Zhang L H, Liu Z K, Zhang Z Y, Zhu Z H, Gao W, Guo G C, Ding D S and Shi B S 2022 *Phys. Rev. Appl.* **18** 014045
[16] Sedlacek J A, Schwettmann A, Kübler H and Shaffer J P 2013 *Phys. Rev. Lett.* **111** 063001
[17] Jiao Y C, Hao L P, Han X X, Bai S Y, Raithel G, Zhao J M and Jia S T 2017 *Phys. Rev. Appl.* **8** 014028
[18] Gordon J A, Simons M T, Haddab A H and Holloway C L 2019 *AIP Advances* **9** 045030
[19] Holloway C L, Simons M T, Gordon J A and Novotny D 2019 *IEEE Antennas Wirel. Propag. Lett.* **18** 1853
[20] Liu Z K, Zhang L H, Liu B, Zhang Z Y, Guo G C, Ding D S and Shi B S 2022 *Nat. Commun.* **13** 1997
[21] Holloway C L, Gordon J A, Schwarzkopf A, Anderson D A, Miller S A, Thaicharoen N and Raithel G 2014 *Appl. Phys. Lett.* **104** 244102
[22] Fan H Q, Kumar S, Daschner R, Kübler H and Shaffer J P 2014 *Opt. Lett.* **39** 3030
[23] Jing M Y, Hu Y, Ma J, Zhang H, Zhang L J, Xiao L T and Jia S T 2020 *Nat. Phys.* **16** 911
[24] Simons M T, Haddab A H, Gordon J A and Holloway C L 2019 *Appl. Phys. Lett.* **114** 114101
[25] Prajapati N, Robinson A K, Berweger S, Simons M T, Artusio-Glimpse A B and Holloway C L 2021 *Appl. Phys. Lett.* **119** 214001
[26] Gao Y C, Ren Y H, Yu D M and Qian J 2019 *Phys. Rev. A* **100** 033823
[27] Carr C, Tanasittikosol M, Sargsyan A, Sarkisyan D, Adams C S and Weatherill K J 2012 *Opt. Lett.* **37** 3858
[28] Thaicharoen N, Moore K R, Anderson D A, Powel R C, Peterson E and Raithel G 2019 *Phys. Rev. A* **100** 063427
[29] Prajapati N, Bhusal N, Rotunno A P, Berweger S, Simons M T, Artusio-Glimpse A B, Wang Y J, Bottomley E, Fan H Q and Holloway C L 2023 *J. Appl. Phys.* **134** 023101
[30] Berman P R and Malinovsky V S 2011 *Principles of Laser Spectroscopy and Quantum Optics* (Princeton: Princeton University Press)
[31] Kondo J M, Šibalić N, Guttridge A, Wade C G, De Melo N R, Adams C S and Weatherill K J 2015 *Opt. Lett.* **40** 5570
[32] Mandel L and Wolf E 1995 *Optical Coherence and Quantum Optics* (Cambridge: Cambridge University Press)
[33] Cai M H, You S H, Zhang S S, Xu Z S and Liu H P 2023 *Appl. Phys. Lett.* **122** 161103